PHYSICAL REVIEW B VOLUME 16, NUMBER 4 15 AUGUST 1977

X-ray studies of $2k_F$ and $4k_F$ anomalies in tetrathiafulvalene-tetracyanoquinodimethane (TTF-TCNQ)

S. K. Khanna,*† J. P. Pouget, and R. Comes
Laboratoire de Physique des Solides,‡ Université Paris-Sud, 91405 Orsay, France

A. F. Garito and A. J. Heeger
Department of Physics,† Laboratory for Research on the Structure of Matter, University of Pennsylvania, Philadelphia, Pennsylvania 19174

(Received 23 December 1976)

X-ray diffuse-scattering studies on tetrathiafulvalene-tetracyanoquinodimethane (TTF-TCNQ) above the 54-K phase transitions reveal two types of one-dimensional scattering at the wave vector $0.295b^*$ (earlier assigned to the $2k_F$ wave vector) and at $0.59b^*$ (corresponding to twice the former wave vector) which can be attributed to two different anomalies in the phonon dispersion spectrum. Both act as precursor effects for the lower-temperature modulated phases. The two anomalies are remarkably different in their temperature dependence and the polarization of the involved phonon modes. The larger wave-vector anomaly ($4k_F$) is already visible at room temperature, sharpens slowly when the temperature is decreased, and condenses at a temperature lower than 54 K. The anomaly at $0.295b^*$, on the contrary, only becomes visible below 150 K, sharpens rapidly with decreasing temperature, and is the first to condense at 54 K into the earlier reported $2a \times 3.4b \times c$-modulated lattice. The $0.295b^*$ anomaly corresponds to a polarization with a longitudinal component along b^* and a transverse component along c^*. The $0.59b^*$ anomaly on the contrary has a strictly longitudinal polarization directed along b^*. The occurrence of both polarizations (b^* and c^*) does not affect the interpretation in terms of charge-density waves, as both of these components modify the intermolecular spacing in chain direction because of the tilt angle of the molecules in the stacks. In agreement with independent experimental data, it is suggested that the 54-K phase transition is due to the condensation of the transverse component of the $2k_F$ anomaly, while the 49-K phase transition corresponds to the condensation of both longitudinal anomalies ($2k_F$ and $4k_F$).

I. INTRODUCTION

The discovery of real physical systems exhibiting the properties of quasi-one-dimensional metals have attracted considerable attention because of the well-known instabilities associated with a one-dimensional (1-D) electron gas.[1,2] Much progress has been made toward clarification of the general trends of the experimental properties of 1-D conductors from the investigations of the prototype Krogmann salt $K_2Pt(CN)_4Br_{0.30} \cdot xH_2O$ (KCP).[3] This compound has indeed the appealing feature of possessing only one type of conducting stack, and should therefore exhibit the simplest genuine properties of such 1-D systems. However, as in the case for all the other presently known single-stack conductors, KCP has a built-in disorder which complicates a detailed understanding of its properties.[1] The only known well-ordered 1-D conductors are the organic charge transfer salts, which by definition possess two different types of conducting stacks and therefore much richer properties. However, the two-stack systems are more complex and require detailed study in order to unravel the respective contributions from each type of stack. The most recent investigations on tetrathiafulvalene-tetracyanoquinodimethane (TTF-TCNQ) are particularly relevant in this respect.

TTF-TCNQ crystallizes indeed in regular segregated stacks of TCNQ acceptors and TTF donors.[4] A series of dc electrical transport,[5] microwave,[6] and optical studies[7] have clearly established the 1-D properties of TTF-TCNQ in the metallic state. From the earliest data, it was suggested that the behavior of TTF-TCNQ was associated with a Peierls instability of the 1-D metallic system, in which a phonon mode is driven soft by the divergent response of the electron gas at the wave vector $q = 2k_F$.[8] Since the initial x-ray diffuse-scattering reports[9] of the existence of the expected low-temperature modulated lattice and Peierls transition in TTF-TCNQ, there have been a number of important studies of the structural properties performed both with neutron scattering and x-ray scattering which have in particular characterized several low-temperature phases and shed some light on the high-temperature precursors.[10-15]

The structural studies have now established that TTF-TCNQ undergoes a sequence of three successive phase transitions at 54, 49, and 38 K, respectively. The 54-K phase transition coincides in particular with the rapid drop of the electrical conductivity[5]; it is believed to be the metal-insulator transition to a high-dielectric-constant

semiconductor,[6] but the successive phase transitions which possibly correspond to the successive ordering of the two different molecular stacks[16,17] might alter this interpretation. The 38-K transition, which was first suggested from high-pressure experiments,[18] was determined to be of first order with the surprisingly large hysteresis of 1° at such low temperatures.[10] The 49-K phase transition is a more subtle one; it was only predicted from a "two chain" Ginsburg-Landau analysis[19] of the initial data,[10] and clearly established from additional high-resolution neutron scattering experiments.[11] Subsequent NMR experiments on ^{13}C-labeled molecules[17] and dc conductivity experiments have further observed anomalies around 49 K.[20] Very recent specific-heat anomalies[21] which have extended the earlier data[22] have further clearly revealed anomalies at 54, 49, and 38 K, giving an unambiguous experimental confirmation that we deal with three real phase transitions in the full sense of such a term.

This sequence of phase transitions has been approached theoretically in terms of two chain models[19,23] in which the two different types of stacks become modulated at different temperatures. Such descriptions have already received some experimental support,[16,17] but a clear confirmation from a structural analysis is still lacking because of the difficulties involved in collecting sufficient data.

These experimental difficulties due to weak intensities are even greater above 54 K. In the earlier x-ray diffuse-scattering measurements, the 1-D precursor effects, attributed to the $2k_F$ giant 1-D Kohn anomaly, were barely observable and only briefly described. Subsequent very careful inelastic neutron scattering experiments[12,14] have succeeded, in spite of the unfavorable conditions imposed by the size of the available single crystals, in clearly establishing the existence of a phonon anomaly at the wave vector $q = 2k_F = 0.295b^*$, occurring surprisingly in a transverse-acoustic branch and only developing well below 150 K. The apparent very sharp longitudinal phonon anomaly at room temperature reported in a previous independent investigation[24] is now attributed to a completely different effect arising from spin-density wave excitations.[25] These neutron scattering measurements could however be performed in only one Brillouin zone because of the very tight intensity conditions, so the 1-D nature of the phonon anomaly was therefore only assumed. The convincing evidence of this 1-D character was shown in two independent recent x-ray investigations, respectively, performed by photographic methods[13] and counter detection.[15] The improved experimental conditions further revealed the existence of an additional 1-D precursor scattering at the wave vector $q' = 4k_F = 0.59b^*$ (or $0.41b^*$ in the reduced zone) which was shown to be an additional genuine and puzzling feature observed to date only in TTF-TCNQ.

The purpose of the present paper is to give a detailed report of the x-ray diffuse-scattering photographic investigation of TTF-TCNQ. After a description of the experimental conditions and difficulties, the results are presented with emphasis on the study of the high-temperature precursor effects in Sec. III (Figs. 1–8), and with useful complementary informations on the low-temperature modulated phases in Sec. IV (Figs. 9 and 10). The results are discussed in Sec. V (Figs. 11–13), and concluding remarks are given in Sec. VI.

II. EXPERIMENTAL

As in the previous x-ray investigations of TTF-TCNQ, the present study was carried out with the fixed film, fixed crystal method, the principle of which is briefly described elsewhere.[26] Since the earlier x-ray study,[9] the experimental efficiency has been considerably improved. The original aluminium window of our x-ray camera was replaced by a less absorbing large-size beryllium window, allowing the use of the more intense Cu $K\alpha$ radiation ($\lambda = 1.54$ Å), instead of Mo $K\alpha$ (0.709 Å) used in the preceding study. Such a higher wavelength is more suitable for the study of weakly absorbing material such as TTF-TCNQ, which in addition has relatively large lattice constants. The cryocooled low-temperature camera, originally built for the use of planar films, was transformed into a cylindrical one, and the beryllium window consequently was cylindrically bent. This cylindrical camera allowed observations at larger scattering angles (up to 130° in the equatorial plane), where the intensity is higher if due to displacive correlations, as expected from phonon anomalies. The initial doubly bent lithium fluoride monochromator was replaced by a doubly bent UCAR (Union Carbide Corp.) pyrolitic graphite monochromator having higher reflectivity [(002) reflections]. The collimation was selected to give the highest possible intensity with an acceptable resolution of about 0.04 $Å^{-1}$ around a 60° scattering angle, as was determined from measurements on powder samples. These modifications resulted in an effective gain in intensity by a factor of the order of 25, which was obtained by comparing the exposure times needed to get patterns comparable in intensity with the earlier investigations.

A semiquantitative analysis of the intensity of

the 1-D diffuse scattering was carried out using a Joyce-Loeble microdensitometer. The extreme weakness of the diffuse streaks, compared to the film background (mainly due to the unperturbed phonons), necessitated the use of a strong absorbing filter on the reference beam of this instrument. With this setup, the cleanest parts of a series of temperature-dependent patterns could be usefully scanned to yield readings such as those shown in Figs. 2 and 8.

The temperature was lowered using a CTI "cryodyne cryocooler," and regulated within 0.2 K. However, the determination of the absolute temperature of the sample itself was difficult at the lower and higher limits of the experimental temperature range (10–300 K). The TTF-TCNQ sample was glued with silver paint on the cryocooler cold finger centered on the axis of the cylindrical camera. In order to avoid parasitic scattering, the photographic film was directly placed on the beryllium window; for the same reason, no thermal screen could be placed between the cooled sample and the beryllium window which was at room temperature. As a consequence, a substantial difference between the temperature measured at the massive cold finger and the actual sample temperature was observed. Using the well-studied 54-K transition of TTF-TCNQ, the temperature could be calibrated by the onset of the satellite superlattice reflections with a precision of about 0.5 K. This calibration allowed an acceptable determination of the sample temperature around 54 K, but prevented accurate measurements concerning the modification of the modulated lattices between 54 and 38 K. At 54 K, an error of several degrees in the absolute temperature was found. This error, decreasing with increasing temperature, will not affect substantially the conclusions concerning the general temperature dependence of the 1-D scattering.

High-quality, untwinned crystals (typically $6 \times 1 \times 0.10$ mm), identical to the ones used in the previous x-ray and neutron studies, were used. Several 100% deuterated, as well as normal protonated single crystals, showed identical results.

III. EXPERIMENTAL RESULTS ON THE HIGH-TEMPERATURE PRECURSORS

A. 1-D regime, $T > 60$ °K

Figure 1(a) shows a diffuse x-ray scattering pattern taken at 60 K. Besides the usual broad spots due to small wave-vector acoustic phonons and some well defined Bragg reflections, two kinds of diffuse lines are clearly visible. They originate from intensity at reciprocal points located in two

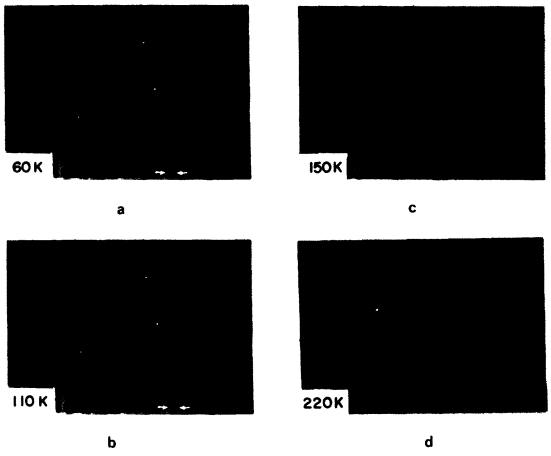

FIG. 1. Diffuse x-ray patterns of TTF-TCNQ in the undistorted conducting phase ($T > 54$ K). The sample is oriented with the b^* and c^* directions in the equatorial plane, the angle between the incident x-ray beam and b^* being 124°. The rings observed around the incident beam are powder parasites from the sample holder. Bragg spots with $0.5\,b^*$ components are due to the $\frac{1}{2}\lambda$ contamination from the continuous spectrum of the x-ray source, which is also reflected by the monochromator. (a) 60 K: The satellite diffuse sheets are clearly visible at the wave vectors $(0.295 \pm 0.02)\,b^*$ identified as $2k_F$ (black arrows) and $(0.59 \pm 0.02)b^*$, the latter corresponding to $0.41b^*$ in the reduced zone, identified as $4k_F$ (white arrows); (b) 110 K: The $2k_F$ scattering has decreased in intensity and is broadened, whereas the $4k_F$ scattering remains sharp; (c) 150 K: The $2k_F$ scattering is undetectable by eye and only $4k_F$ scattering is visible; (d) 220 K: The $4k_F$ scattering is still clearly visible.

different sets of satellite sheets. One set, indicated by black arrows, has a wave-vector component in chain direction of $q = 0.295b^*$ earlier assigned to $2k_F$ and corresponds to the previously reported Kohn anomaly. Another set, indicated by white arrows, has a wave-vector component in chain direction of $0.41b^*$ (or $0.59b^*$ in the extended zone), that is to say, twice the wave vector of the former set and therefore assigned to $4k_F$.[13,15]

The photographic patterns of Fig. 1 show that both the $2k_F$ and $4k_F$ scattering increase in intensity with increasing scattering angle, demonstrating that they both arise from displacive modulations of the TTF and TCNQ molecular positions.

Both the $2k_F$ and $4k_F$ scatterings appear as interrupted diffuse lines unlike the continuous diffuse lines observed in the case of the 1-D platinum conductor KCP.[1,2,26] Closer inspection of Fig. 1 shows the intensity of the diffuse sheets follows substantially the intensity distribution of the Bragg peaks (or acoustic phonon clouds) from the undistorted 3-D main lattice. This correlation shows that the intensity distribution of the 1-D scattering follows the form factor of the TTF and TCNQ molecules.

1. Temperature dependence of the $2k_F$ and $4k_F$ scattering

As observable in Fig. 1(a), around 60 K, both the $2k_F$ and $4k_F$ scatterings are sharp and of comparable intensity. These common features are however progressively lost when the temperature is increased.

With increasing temperature, the $2k_F$ scattering progressively broadens in the chain direction and rapidly decreases in intensity as is clearly shown in the pattern of Fig. 1(b) taken at 110 K. Above 150 K [Figs. 1(c) and 1(d)], the $2k_F$ scattering is no longer detectable by eye. Microdensitometer readings of such photographic patterns are extremely difficult to obtain because of the high background. It is only in a clean and low background area corresponding to the $(\bar{4}12)$ zone, that a series of patterns over the temperature range 60–300 K could be usefully scanned. The results are illustrated in the representative scans of Fig. 2, which give a more quantitative measure of the temperature dependence of the diffuse scattering. It is remarkable that above 150 K (scans at 180, 240, and 300 K), a weak break in the slope of the scattering at about the same wave vector as the low-temperature $2k_F$ scattering is clearly visible. The microdensitometer scans shown in Fig. 2, and in particular the subsistence of a very weak $2k_F$ anomaly up to room temperature, is in excellent agreement with the independent x-ray counter investigation.[15]

On the other hand, the $4k_F$ scattering shows an entirely different behavior. It remains relatively sharp and intense up to room temperature as shown in the patterns of Figs. 1(c) and 1(d), and further shifts slightly in position; these features are clearly observable in Fig. 2.

A semiquantitative analysis can be performed from such microdensitometer scans of the photographic patterns. This provides an evaluation of the 1-D scattering relative to the background which is mainly due to the unperturbed phonons. If the assumption is made that the 1-D scattering arises solely from dynamical anomalies in the phonon spectrum, the associated intensity maximum relative to the background is proportional to $k_B T(1/\omega^2 - 1/\omega_0^2)$, where ω_0 and ω are the frequencies of the bare and renormalized phonons, respectively (this neglects all other phonons except one branch showing an anomaly). The temperature dependences of the intensity maxima of the $2k_F$ and $4k_F$ scatterings which are obtained at the points $(-3.6a^*, 2.705b^*, 2.05c^*)$ and $(-3.6a^*, 2.41b^*, 1.25c^*)$ are shown together in Fig. 3, showing more precisely the very different behavior of the two types of 1-D scattering. These differences are also reflected in the temperature dependences of the HWHM [half width at half maximum in chain direction of the $2k_F$ and

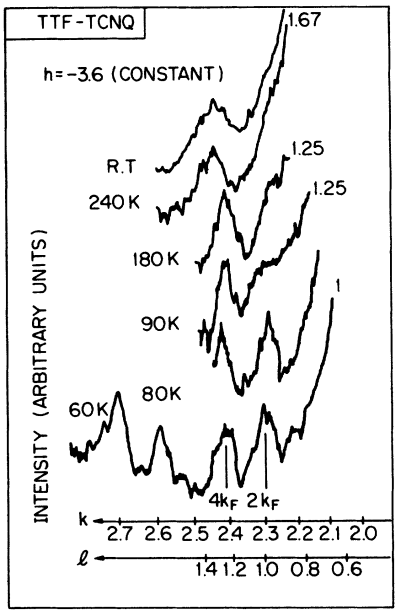

FIG. 2. Microdensitometer scans of the $2k_F$ and the $4k_F$ scattering intensities at several temperatures. The h, k, l, values corresponding to the scans are indicated on the figure. The scans clearly demonstrate the rapid decrease in the intensity and the broadening of the $2k_F$ scattering between 60 and 300 K; a very weak anomaly still persists up to room temperature in the vicinity of $2k_F$. The intensity of the $4k_F$ scattering has much less temperature dependence, but there is a slight shift in the position in the two higher temperature scans; this shift is in agreement with the x-ray counter investigation (Ref. 15). The numbers on the right-hand side of the higher-temperature scans are normalizing factors in order to scale with the lower-temperature readings.

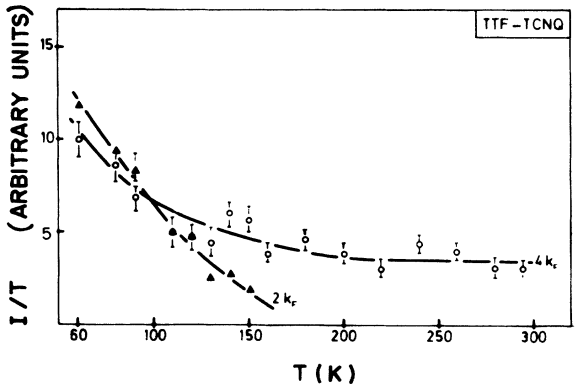

FIG. 3. Temperature dependence of the peak intensity of the $2k_F$ and the $4k_F$ scatterings recorded by microdensitometer at the points (−3.6, 2.705, 2.05) and (−3.6, 2.41, 1.25). The ordinate is plotted as $1/T$ in order to eliminate the temperature dependence of the phonon population factor, which is proportional to kT for low-frequency phonons.

$4k_F$ scatterings (Fig. 4)]. With a Lorentzian resolution correction, the inverse HWHM yields a correlation length along the chains direction of approximately 100 Å near 60 K for both types of scattering. For the $4k_F$ scattering, this value decreases slowly with increasing temperature to approximately 9 Å at room temperature. The $2k_F$ correlation length decreases rapidly to approximately 5 Å near 150 K, becoming immeasurably small at higher temperatures.

Within experimental error ($\pm 0.02b^*$), the position of the $2k_F$ diffuse sheet (wave vector equal to $0.295b^*$) is temperature independent below 150 K. Above 150 K, if the break in the slope of the background scattering visible in Fig. 2 clearly shows the existence of a weak $2k_F$ scattering, its precise position cannot be determined. This impossibility reflects the physical fact that a weak intensity is likely to arise from a broad anomaly, as observed for instance by neutron scattering in the longitudinal phonon branch and around $0.295b^*$.

In the case of the $4k_F$ scattering, the position can be followed up to room temperature. It is found that the wave vector in the chain direction changes from the low-temperature value $0.41b^*$ to $0.45b^*$ at room temperature, in agreement with the x-ray counter measurements.[15] Figure 5 further suggests this change occurs in the temperature region around 200 K, calling for detailed studies of the electronic properties in this temperature range.

2. *Polarization of the $2k_F$ and $4k_F$ scattering*

The patterns of Fig. 1 clearly show, as already mentioned, that the diffuse scattering arises from displacive modulations. However, these patterns alone do not provide a unique assignment of the polarization components of the displacive modulations. This question of the polarization of the atomic displacements involved in the charge density waves of TTF-TCNQ is somewhat unclear from the previous studies. Preliminary structure factor calculations on the low-temperature $2k_F$ satellites ($T < 38$ K) first suggested the presence of both longitudinal and transverse (c^*) components for the $2k_F$ modulations.[10] The already mentioned inelastic neutron measurements simultaneously clearly demonstrated the development of a sharp $2k_F$ phonon anomaly below 150 K in the transverse (c^*) branch for phonons propagating in chain direction, but also the existence of a shallow $2k_F$ anomaly in the longitudinal branch at room temperature which could not be followed towards lower temperature because of lacking intensity.[12,14] The x-ray counter investigation which covered both the $2k_F$ and $4k_F$ scattering concluded that the $2k_F$ scattering had mainly a transverse (c^*) polarization, while the $4k_F$ scattering appeared to have a strictly longitudinal one.[15] This situation motivated a systematic study of the polarizations of the $2k_F$ and $4k_F$ scatterings in the present measurements, using several characteristic crystal orientations. Figure 6 illustrates for two typical cases the orientation of the reciprocal lattice in the equatorial plane, together with its intersection with the Ewald sphere. Figure 6 easily allows the determination of the scattering vectors $Q = ha^* + kb^* + lc^*$ on the correponding patterns shown in Fig. 7 taken at 60 K.

These patterns, respectively, display principal components of the scattering vector in the b^*-c^* ($0kl$) and b^*-a^* ($hk0$) reciprocal planes. In each pattern, along the vertical b^* axis [$l = 0$ in Fig. 7(a) and $h = 0$ in Fig. 7(b)], both the $2k_F$ and $4k_F$ scattering are directly observed. As the scattered intensity from phonons or any displacive correlations is proportional to $(\vec{Q}\cdot\vec{u})^2$, where $\vec{u}$ is the displacement vector, this establishes the existence of a longitudinal component in chain direction *for each type of scattering.* The comparable intensity of the two types of scattering along the vertical b^*

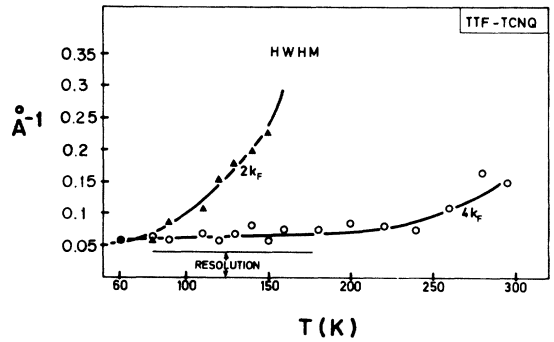

FIG. 4. Temperature dependence of the half width at half maximum (HWHM) for the $2k_F$ and the $4k_F$ scatterings taken from the microdensitometer scans; same as used in Fig. 3.

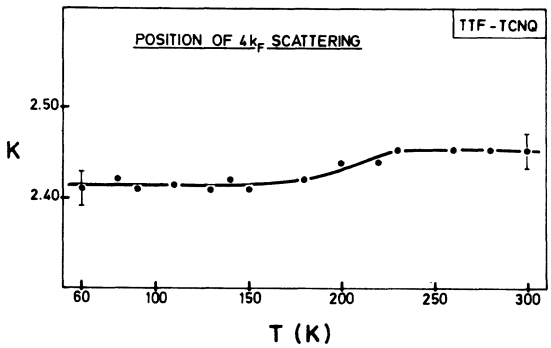

FIG. 5. Temperature dependence of the position of the $4k_F$ scattering. Note that the shift takes place only around 200 K.

axis further indicates similar amplitudes for both longitudinal components at 60 K.

Figure 7(a) reveals in addition that the intensity of the $2k_F$ scattering increases with increasing c^* component of the scattering vector. This is particularly striking for the $2k_F$ sheets which lie closest to the equatorial plane ($0a^*, \pm 0.295b^*, lc^*$) for which the longitudinal component has a negligible contribution to the intensity, thus clearly showing the existence of a transverse c^* component of the polarization of the $2k_F$ scattering. [For phonons propagating along the b^* direction, a symmetry analysis shows that one can separate the spectrum between pure longitudinal and transverse modes. But this analysis cannot fix a particular direction for the polarization of the transverse modes. The experimental results show only that the $2k_F$ transverse anomaly has a polarization quite close to the c^* or c direction. In the 1-D regime, a c^* direction, which is situated in the plane of symmetry of the molecular chains, seems more likely for the transverse-acoustic modulation of the intermolecular spacing, than a c direction (see Fig. 12).]

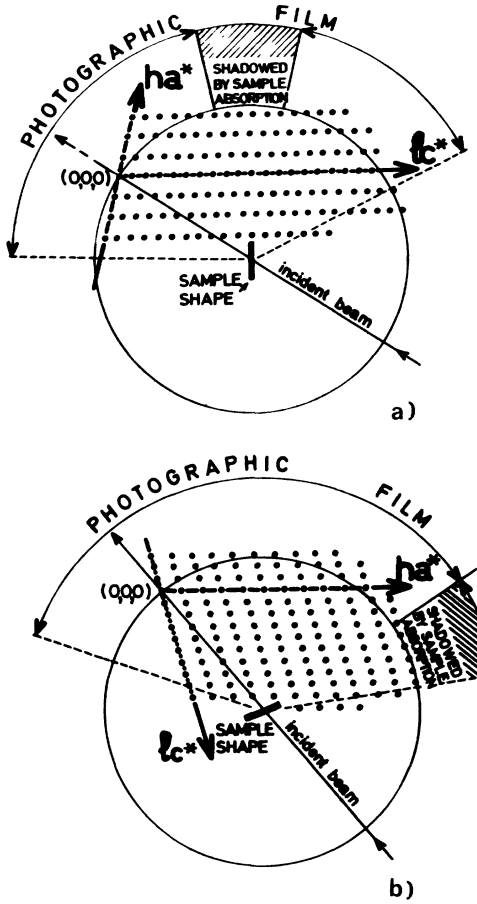

FIG. 6. Schematic representation of the reciprocal lattice in the equatorial plane ($h0l$) and its intersection with the Ewald sphere for the crystal orientations used in determining the polarization of the $2k_F$ and $4k_F$ scatterings. (a) The reciprocal-lattice points intersecting the sphere correspond to a wide range variation of l values (in the c^* direction), but only restricted variation of h values (along a^*); (b) The reciprocal-lattice points intersecting the Ewald sphere correspond to a wide range variation of h values (in a^* direction), but only restricted variation of l values (along c^*).

No such intensity dependence upon the c^* component of the scattering vector is observed for the $4k_F$ scattering. Figure 7(b) further shows that neither the $2k_F$ nor the $4k_F$ scattering exhibits any detectable intensity increase with increasing a^* component of the scattering vector. These results demonstrate unambiguously that the $4k_F$ scattering is purely longitudinal, while in addition to the longitudinal b^* component the polarization of the $2k_F$ scattering has a transverse component along c^*. The existence of two components of the polarization for the $2k_F$ scattering is consistent with the inelastic neutron data.[12]

Similar measurements performed at different temperatures show that both longitudinal and trans-

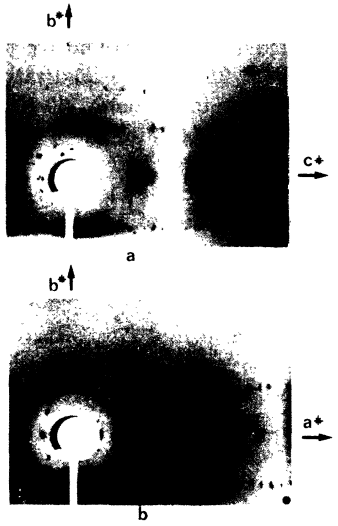

FIG. 7. Diffuse x-ray patterns of TTF-TCNQ taken at 60 K for the two different orientations of Fig. 6. Along the vertical b^* axis [$l = 0$, no c^* component of the scattering vector in Fig. 7(a) and $h = 0$, and no a^* component of the scattering vector in Fig. 7(b)], both the $2k_F$ and $4k_F$ scatterings can be observed showing the existence of a longitudinal component (along b) of the polarization for the $2k_F$, as well as the $4k_F$ scatterings. (a) With increasing l (c^* direction), only the $2k_F$ scattering intensity increases. This is, in particular, striking close to the equatorial layer line where the b^* longitudinal component contributes only negligibly. (b) Neither $2k_F$ nor $4k_F$ scatterings exhibit an increase in intensity for increasing h (along a^*), showing the absence of any substantial a^* component of their polarization.

verse components of the $2k_F$ scattering decrease with increasing temperature above 60 K and become undetectable by eye above 150 K as already mentioned. From the x rays alone, it is therefore not possible to determine the polarization of the weak $2k_F$ scattering which remains up to room temperature (Fig. 2) the inelastic neutron scattering data alone seems to indicate a strictly longitudinal polarization.

The intensity of the $2k_F$ and $4k_F$ diffuse scattering relative to the main Bragg peaks could not be measured accurately in the present study. An indirect estimation[13] yields a ratio of the diffuse-scattering intensity compared to the closest main Bragg reflections of about 10^{-6} at 60 K for both scatterings, and of about 10^{-7} at 130 K for the $2k_F$ scattering. This last figure sets also an order of magnitude of our detectability. Applied to the determination of the polarization of the scattering, this shows that other contributions than shown above,[27] if they exist, must be at least an order of magnitude smaller than the longitudinal components at 60 K.

B. Onset of 3-D order: $54 < T < 60$ K

In the temperature range near 60 K, the diffuse-scattering sheets at $2k_F$ change qualitatively. The photographic patterns taken below 60 K show directly the progressive building up of the diffuse sheets into satellite spots corresponding to a wave vector $(0.5a^*, 0.295b^*, 0c^*)$. Figure 8 gives the microdensitometer traces of a $2k_F$ sheet along the a^* direction for a series of patterns close to 54 K. The progressive buildup of the satellite spots when approaching 54 K is clearly seen. In this temperature range, no significant changes take place in the $4k_F$ diffuse scattering which maintains its 1-D character.

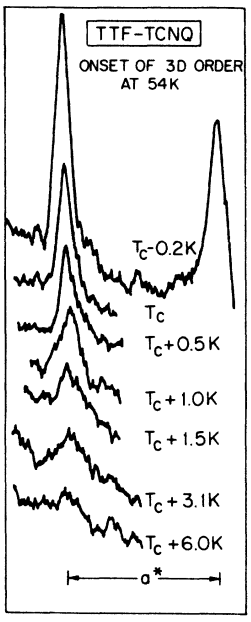

FIG. 8. The microdensitometer scans in the $2k_F$ plane along the a^* direction, showing the onset of 3-D order close to 54 K, and the corresponding formation of the (3.5, 3.295, 3) satellite. Two successive satellites of the $2k_F$ plane in the a^* direction have been recorded just below the phase transition in order to provide a scale (see the insert in the pattern of Fig. 9).

The 3-D coupling between the chains, as evidenced by the buildup of satellite spots, begins just below 60 K, where the electrical conductivity exhibits its maximum value. Below 58 K, the decrease of the electrical conductivity might be explained by the progressive setting of the interchain phase relation (growth of the transverse coherence) and the associated destruction of the 1-D fluctuation effects.

At 54 K, within the resolution limits (about 0.04 $Å^{-1}$) of this investigation, and in agreement with previous studies, long-range 3-D order is achieved as far as the $2k_F$ satellites are concerned.

IV. EXPERIMENTAL RESULTS ON THE 3-D MODULATED PHASES

As briefly mentioned in the introduction of this paper, previous studies have clearly established and characterized three different low-temperature modulated phases in TTF-TCNQ. The experimental technique (fixed crystal, fixed film) used in the present study is not well adapted for a detailed investigation of very localized scattering such as superstructure satellites, and the difficulties already mentioned above related to the precise determination of the absolute sample temperature would moreover lead to very inconclusive results. We shall therefore only briefly describe a few specific points.

The photographic patterns in Figs. 9 and 10, taken at 50 and 30 K, respectively, demonstrate the consistency between the present results and the earlier work.[9-15] In the pattern of Fig. 9, which corresponds to the modulated phase stable between 54 and 49 K, no $4k_F$ satellites can be observed, but arrays of $2k_F$ satellites are clearly visible. These satellites are found at positions $((h \pm 0.5)a^*, (k \pm 0.295)b^*, lc^*)$, where hkl are the integer Miller indices referring to the high-temperature undistorted lattice. This corresponds to the modulation $2a \times 3.40b \times c$. Such series of satellites confirm the reality of this phase, which in the previous counter studies was established from measurements restricted on only one such satellite. A closer inspection of the pattern of Fig. 9 reveals that all visible $2k_F$ satellites correspond to positions with a nonzero scattering vector component in c^* direction $(l \neq 0)$, this particular point in connection with other data suggests further comments on the possible mechanism of the successive phase transition at 54 and 49 K, and will be developed in Sec. V.

The pattern shown in Fig. 10, taken at 30 K,

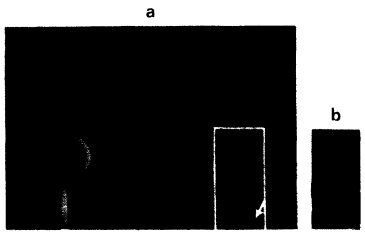

FIG. 9. (a) Diffuse x-ray pattern of TTF–TCNQ at 50 K (modulated phase I). The sample is oriented in the reciprocal equatorial plane $(0kl)$, the angle between the incident x-ray beam and the b axis being 125°. Note that besides the well-defined $2k_F$ arrays of weak satellites with wave-vector components $(0.5a^*, 0.295b^*, 0c^*)$, sharp 1-D $2k_F$ scattering persists at this temperature. The $4k_F$ scattering retains its 1-D character at this temperature (no $4k_F$ satellites). As in the patterns of Fig. 1, Bragg spots with $0.5b^*$ components must be disregarded, as they arise from $\frac{1}{2}\lambda$ contamination. In the insert, the black arrow points toward the (3.5, 3.295, 3) satellite, where the onset of the 3-D order was measured (see Fig. 8), the white arrow points toward the (4.5, 3.295, 5) satellite. (b) The same region as the insert is shown at 55 K, where the two satellites are clearly broadened.

shows two types of satellites with $2k_F$ and $4k_F$ wave vector components in chain direction. The first series of $2k_F$ satellites are found at the positions $((h \pm 0.25)a^*, (k \pm 0.295)b^*, lc^*)$ corresponding to the $4a \times 3.40b \times c$ modulated lattice stable below 38 K. An interesting point to note is that a few satellites with zero scattering vector component in c^* direction $(l = 0)$ are now visible, in agreement with previous neutron scattering data,[10] and in contrast with the observations made above about the pattern of Fig. 9.

The second series of $4k_F$ satellites revealed in Fig. 10 are all found at wave vectors which are twice those of the $2k_F$ satellites, corresponding to the positions $((h \pm 0.50)a^*, (k \pm 0.41)b^*, lc^*)$. No

FIG. 10. Diffuse x-ray pattern of TTF-TCNQ at 30 K. The sample is oriented in the reciprocal equatorial plane $(0kl)$, the angle between the incident x-ray beam and b^* axis being 124°. Both the $2k_F$ and the $4k_F$ scatterings are condensed into satellite spots at the wave vectors $(0.25a^*, 0.295b^*, 0c^*)$ and $(0.5a^*, 0.41b^*, 0c^*)$, respectively. Horizontal arrows point toward the $2k_F$ (4.25, 2.295, $\bar{1}$) and (3.75, 2.705, 0) satellites, vertical arrows point toward the $4k_F$ (3.5, 2.41, $\bar{1}$) and (4.5, 2.59, 0) satellites.

$4k_F$ satellites could be observed at the positions $(ha^*, (k \pm 0.41)b^*, lc^*)$, also mentioned in the x-ray counter investigations.[15]

In the intermediate phase $38 < T < 49$ K, in which the positions of both sets of satellite vary strongly with temperature, we found good agreement with the previous studies[9-15]; in particular, the $4k_F$ satellites could be observed up to 45 K, at wave vectors which remained twice those of $2k_F$ satellites.

Figure 11 summarizes schematically the positions of the satellites in the three low-temperature phases consistently obtained from the different investigations.

As a concluding remark on the results concerning the low-temperature phases, it is noteworthy that the $4k_F$ satellites are generally weak and always found at twice the wave vector of the $2k_F$ ones. Generally, these low-temperature $4k_F$ superlattice reflections could arise either as second-order diffraction harmonic of the $2k_F$ ones, or they could result from additional secondary distortion, whose wave vector is locked at a second-harmonic value by nonlinear coupling with the primary $2k_F$ distortion. Therefore, in this last possibility, their presence does not modify the symmetry of the earlier established low-temperature modulated *lattices*, but should alter only the atomic displacements. However, it should be noticed that the formation of $4k_F$ low-temperature satel-

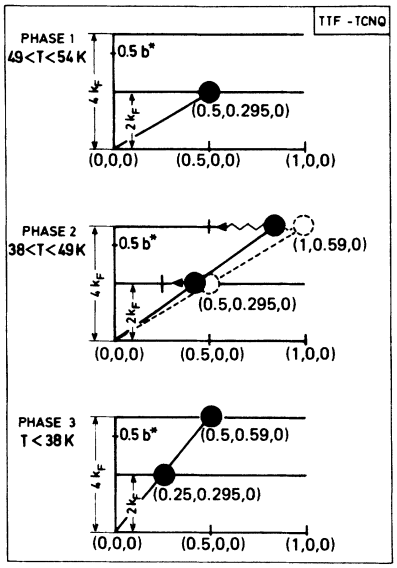

FIG. 11. Schematic representation of the position in reciprocal space of the satellite spots in the three low-temperature modulated phases. (a) $49 < T < 54$ K (phase I)—modulation $2a \times 3.4b \times c$; (b) $38 < T < 49$ K (phase II)—modulation $\times (T)a \times 3.4b \times c$; (c) $T < 38$ K (phase III)—modulation $4a \times 3.4b \times c$.

lite spots as second-order diffraction harmonic of the $2k_F$ ones is in contrast with the high-temperature observations on the 1-D precursors, and a direct comparison between the intensity of the superlattice satellite spots must take the different polarizations of the $2k_F$ and $4k_F$ precursors into consideration. For instance, it is by no means established that the $4k_F$ satellites, which can be assumed to arise from a longitudinal modulation, are weaker in intensity than the fraction of the intensity of the $2k_F$ satellites arising from their longitudinal component alone. (In fact, some counter measurements on few satellites[11,15] give comparable intensities between the $4k_F$ satellites and the $2k_F$ satellites without l components.) This gives some confidence in the other interpretation, where the $4k_F$ satellites represent intrinsic distortions in the low-temperature phases. This will be further discussed in Sec. V.

V. DISCUSSION

A few relevant comments on restricted points of the experimental results were already made in Secs. I–V. We can therefore focus this discussion on the two most important aspects: the unusual polarization of the displacive modulations and the existence of two different precursors.

The results from the photographic patterns given in Fig. 7 establish the unusual feature for the $2k_F$ Kohn anomaly that there are both longitudinal (b^*) and transverse (c^*) components of the molecular motions. One possibility for this polarization behavior can be understood by referring to the schematic representation of the molecular packing of the crystallographic structure [Fig. 12(a)]. Since the molecular planes are tilted, with respect to the crystallographic b stacking axis, around the a direction, the intermolecular spacing can be modulated simultaneously by a longitudinal component and a transverse component perpendicular to the a direction (the latter direction corresponds to the reciprocal c^* axis). These modulations are schematically represented in Fig. 12(b), in the approximation that the molecules are modulated as rigid units. This is consistent with a $2k_F$ charge-density wave arising from the modulation of the intermolecular spacing.

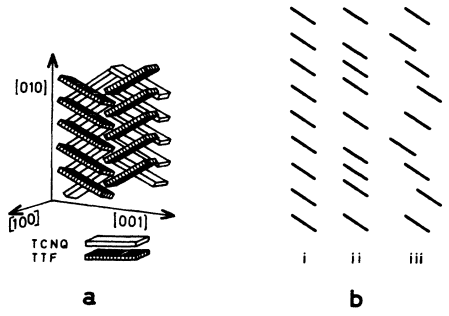

FIG. 12. (a) Schematic representation of the stacking of the TCNQ and TTF molecules. Note that the molecular plane is not perpendicular to the stacking b direction, but is tilted around the a axis of the unit cell. (b) Schematic representation of the intermolecular spacing of the tilted molecules: (i) without modulation; (ii) with longitudinal modulation; (iii) with transverse modulation.

In light of the previous descriptions of the low-temperature phases and the existing data on the polarization of the atomic motion responsible for the $2k_F$ scattering, one additional element for the understanding of the 54- and 49-K phase transitions can be suggested. Assuming, as was done up to now, that both of these phase transitions are driven by phonon anomalies, a possible mechanism for the two successive phase transitions is that the transverse (c^* polarization) branch anomaly condenses at 54 K, while the second longitudinal branch anomaly (b polarization) condenses at 49 K. This suggests that there are two separate $2k_F$ anomalies. Presently, there is no absolute proof of such a mechanism, but it seems to be consistent with several independent experimental observations: (i) the existence of the shallow $2k_F$ phonon anomaly in the longitudinal branch observed above 200 K, in addition to the sharp transverse branch anomaly observed below 150 K by neutron scattering; (ii) the absence of $2k_F$ satellites with zero scattering vector component along c^* in the phase stable between 54 and 49 K found in the present investigation, which implies that only the transverse (c^*) anomaly is condensed in this phase; (iii) the persistence of strong 1-D $2k_F$ scattering below the 54-K phase transition found in the x-ray studies (see Fig. 9 and Ref. 15), which could be due to the noncondensed longitudinal anomaly; (iv) finally, providing perhaps the strongest experimental evidence, it accounts for the different temperature dependences of the intensity of several satellite Bragg peaks below 54 K, as reported earlier.[10]

Figure 13 reproduces the intensity dependence of these satellites as a function of temperature as measured by elastic neutron scattering.[10] The intensity of the $(\zeta, 1.295, 3)$ satellite which has a c^* wave-vector component persists up to 54 K, while the intensity of the $(1+\zeta, 2.705, 0)$ which has a b^* component, but no c^* component, extrapolates to zero around 49 K. Initially this different behavior was assigned to differences in the structure factor arising from the changing modulation below 49 K. However, subsequent neutron measurements[28] show there are several satellites within the same ($hk0$) zone (that is to say satellites with zero c^* wave-vector components) which have a similar

temperature dependence as the $(1+\zeta, 2.705, 0)$ satellite. This indeed strongly suggests that the b^* component of the $2k_F$ anomaly condenses around 49 K.

If we further consider the $4k_F$ satellites, it is noticeable that the detailed temperature dependence of their intensity and position from the x-ray counter investigation leads to the conclusion that the longitudinal $4k_F$ anomaly also possibly condenses at 49 K or eventually slightly below this temperature.[15]

In other words, these different points seem to make a clear distinction between the transverse (c^*) anomaly ($2k_F$), condensing at 54 K, and the two longitudinal anomalies ($2k_F$ and $4k_F$). From the experimental structural data, it is presently still unclear whether both longitudinal anomalies condense at 49 K or if the longitudinal $2k_F$ condenses alone at 49 K, and the longitudinal $4k_F$ anomaly condenses only at a lower temperature, giving rise to an additional phase transition at 46 K as suggested from recent specific-heat measurements[21] and the theoretical work of Barisic.[29]

It should be emphasized here, that the preceding description is by no means in contradiction with the earlier developed two-chain theories. It rather adds a complementary aspect, and provides some information on the two noninteracting modes which are required for such models.

So far, we have tried to characterize as well as possible, with the existing data, the two different precursors, and their successive condensations into different modulated phases; another and more difficult question is to try to understand their

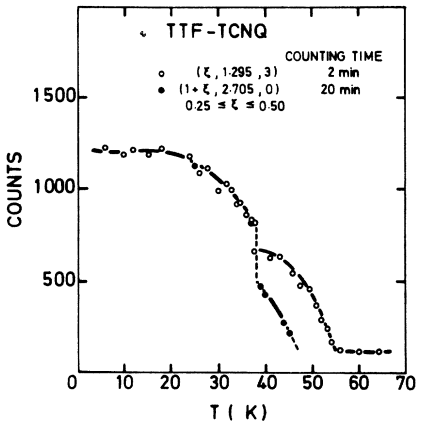

FIG. 13. Temperature dependence of the intensity of two different satellites measured by elastic neutron scattering (Ref. 10). Note that the $(\zeta, 1.295, 3)$ satellite which has an important c^* component persists up to 54 K, while the $(1-\zeta, 2.705, 0)$ satellite which has a b^* component, but no c^* component, extrapolates to zero intensity around 49 K.

physical origins.

Keeping in mind the discussion on the polarizations, a possible origin of the simultaneous occurrence of the $2k_F$ and $4k_F$ anomalies, is to assume that the $2k_F$ transverse anomaly occurs on one of the sets of chains, either TTF or TCNQ, and the longitudinal anomalies ($2k_F$ and $4k_F$) on the other set of chains. The first set of chains behaves as a normal 1-D metal, with possible attractive interactions between electrons, and gives rise to the transverse $2k_F$ Kohn anomaly at the wave vector $0.295b^*$. The second set, owing to particular interactions of the conduction electrons along the chain, exhibits the $4k_F$ anomaly at $0.59b^*$. In such a case among the longitudinal anomalies, it is the $4k_F$ one which is the driving instability, at least at high temperature, in agreement with the relative intensities. Close to the 49-K phase transition, however, the relative role of the two anomalies seems to be reversed and the longitudinal $2k_F$ anomaly has apparently become the driving one, possibly even condensing alone at 49 K, and the $4k_F$ only at a lower temperature.[21] This mechanism seems to be presently the only one consistent with the structural data, the experimental and theoretical evidence in favor of the two-chain models which so well describe the sequence of modulated phases of TTF-TCNQ.

It was already suggested that the particular interactions mentioned above involve repulsive Coulomb interactions between electrons along the chains.[29] Simplest, though schematic, is to use the strong-coupling limit which directly leads to a $4k_F$ anomaly as shown much earlier.[30] It is out of the scope of this experimental paper to go further into theoretical details which are still under intensive investigation.

In the course of this paper, we have followed the earlier assignments of $2k_F$ for the $0.295b^*$ anomaly and satellites, and $4k_F$ for the $0.41b^*$ ($0.59b^*$ in the extended zone) anomaly and satellites. This assignment gives a charge transfer between the TTF and TCNQ molecules of 0.59 electrons, in exceptional agreement with the independent estimations from other type of studies.[31] One should however insist that another assignment such as $2k_F$ for the $0.59b^*$ anomaly and k_F for the $0.295b^*$ cannot be ruled out; it would give a charge transfer closer to one, in favor of which one can also find independent experimental support.[32] It can be further noticed that the idea of the strong-coupling repulsive interactions which are necessary in order to account for the $4k_F$ scattering, have also been challenged in recent work.[33] Up to date however no alternative theory using this second possible assignment for the two types of scattering has been worked out.

VI. CONCLUSION

The present paper has described in relative detail, the results obtained by photographic x-ray measurements on TTF-TCNQ. This work is closely related to the independent x-ray measurements performed by Kagoshima *et al.*[9,5] and the *elastic* neutron scattering studies[10,11] which both used counter detection. The agreement between these different investigations is excellent and reflects the very complementary aspects of the photographic methods and counter measurements. The counter detection is more precise for very localized diffraction and its temperature dependence, such as the satellites of the low-temperature modulated phases.[10,11,15] The photographic method, on the other hand, gives in one pattern a more qualitative but also more general overview of a large section of reciprocal space and therefore provides more information on less localized scattering such as precursor effects, in particular when their location in reciprocal space, or even their existence is unknown prior to the measurements. These specific characters of the photographic methods are clearly outlined by the most important results presented in this paper and in the previous brief reports,[9,13] which can be summarized as follows: (i) the first structural evidence of any phase transition in TTF-TCNQ; (ii) the observation of two different instabilities, namely $2k_F$ and $4k_F$, and, in particular, their purely 1-D nature; (iii) the measure of the progressive buildup of the 3-D coupling between the chains in the temperature range 60–54 K; (iv) the unambiguous determination of the different polarizations of the two anomalies, which together with previous elastic neutron scattering data[10] has lead to the model described here, where the successive phase transitions at 54 and 49 K are driven by two different $2k_F$ anomalies, respectively, on the transverse (c^*) and longitudinal phonon branches; (v) the observation of arrays of satellites in the phase stable between 54 and 49 K, where the counter detection measurements could only be performed on one satellite reflection.[10,15]

Some parts of this study of course overlap with the investigations of Kagoshima *et al.*,[15] in particular, the temperature dependence of both types of precursor effects. There is only one discrepancy between the present work and the x-ray counter study,[15] this concerns the $(ha^*,(k\pm0.41)b^*,lc^*)$ satellite reported below 38 K in the latter, and which we have been unable to observe in any pattern, despite the large section of reciprocal space which were explored.

It is clear that the structural data obtained over the last 18 months have considerably improved the understanding of the exceptional properties of TTF-TCNQ. They are, however, still incomplete from several points of view compared to what is usually obtained for similar x-ray and neutron investigations on more conventional compounds. It may be useful to repeat again here that TTF-TCNQ is an exceptionally difficult case and that we deal with extremely weak effects; most of the experimental results were obtained close to the limits of detection and the exploitable data restricted to a few satellites, or a few Brillouin zones. The successive steps of the structural study have therefore been mostly intuitive, rather than the logical result of a quantitative analysis, leaving open the possibility of many speculations.[27]

There are clearly two important structural aspects which need further studies:

(i) The dynamical properties of both the $2k_F$ and $4k_F$ precursors close to the phase transitions. One may wonder in particular if the $4k_F$ scattering is a real phonon anomaly or rather quasielastic and at which precise temperature it condenses in satellites.

(ii) The determination of the atomic motions corresponding to each type of scattering, and each type of polarization. In this respect, preliminary attempts[13] seem to favor a translational motions of rigid molecules. A detailed analysis of these atomic motions is now under progress.

ACKNOWLEDGMENTS

This work is part of a collaboration and has clearly benefited from many discussions with our colleagues from Brookhaven National Laboratory: W. D. Ellenson, S. M. Shapiro, G. Shirane, and V. Emery. Many discussions with S. Barisic, A Guinier, J. Friedel, and M. Lambert and exchanges of information with S. Kagoshima are also acknowledged.

---

*Permanent address: Dept. of Physics and Laboratory for Research on the Structure of Matter, University of Pennsylvania, Philadelphia, Penn. 19174.

†Work supported in part by the NSF through Grant No. DMR-74-22923 and through the University of Pennsylvania Materials Research Laboratory (DMR-72-03025), and by the Advanced Research Projects Agency through Grant No. DAHC-15-72-C-1074.

‡Associé au CNRS.

[1]In *Lecture Notes in Physics*, edited by J. Ehlers, K. Hepp, and H. A. Weidenmüller (Springer, New York, 1975), Vol. 34; in *Low Dimensional Cooperative Pheno-*

mena, edited by H. J. Keller (Plenum, New York, 1975); A. J. Berlinsky, Contemp. Phys. 17, 331 (1976); J. J. Andre, A. Bieber, and F. Gautier, Ann. Phys. (Paris) 1, 145 (1976).

[2]In *Chemistry and Physics of one Dimensional Metals*, edited by H. J. Keller (Plenum, New York) (to be published); *Proceedings of the Conference on Organic Conductors and Semiconductors*, Siofok (Hungary), 1976 (Springer, Berlin, to be published).

[3]K. Krogmann, Ang. Chem. (Int. Ed. Engl.) 8, 35 (1969).

[4]B. T. Kistenmacher, T. E. Philips, and D. O. Cowan, Acta Crystallogr. B 30, 763 (1974); R. H. Blessing and P. Coppens, Solid State Commun. 15, 215 (1974); A. J. Schultz, G. D. Stucky, R. H. Blessing, and P. Coppens, J. Am. Chem. Soc. 98, 3194 (1976).

[5]J. H. Perlstein, J. P. Ferraris, V. V. Walatka, and D. O. Cowan, AIP Conf. Proc. 10, 1494 (1972); J. P. Ferraris, D. O. Cowan, V. V. Walatka, and J. H. Perlstein, J. Am. Chem. Soc. 95, 948 (1973); L. B. Coleman, M. J. Cohen, D. J. Sandman, F. G. Yamagishi, A. F. Garito, and A. J. Heeger, Solid State Commun. 12, 1125 (1973); M. J. Cohen, L. B. Coleman, A. F. Garito, and A. J. Heeger, Phys. Rev. B 10, 1298 (1974).

[6]S. K. Khanna, E. Ehrenfreund, A. F. Garito, and A. J. Heeger, Phys. Rev. B 10, 2205 (1974); S. K. Khanna, A. F. Garito, A. J. Heeger, and R. C. Jaklevic, Solid State Commun. 16, 667 (1975); M. Cohen, S. K. Khanna, W. J. Gunning, A. F. Garito, and A. J. Heeger, *ibid.* 17, 367 (1975).

[7]A. A. Bright, A. F. Garito, and A. J. Heeger, Solid State Commun. 13, 943 (1973); Phys. Rev. B 10, 1328 (1974); P. M. Grant, R. L. Greene, G. C. Wrighton, and G. Castro, Phys. Rev. Lett. 31, 1311 (1973); D. B. Tanner, C. S. Jacobsen, A. F. Garito, and A. J. Heeger, *ibid.* 32, 1301 (1974); C. S. Jacobsen, D. B. Tanner, A. F. Garito, and A. J. Heeger, *ibid.* 33, 1559 (1974); L. B. Coleman, C. R. Fincher, Jr., A. F. Garito, and A. J. Heeger, Phys. Status Solidi B 75, 239 (1976); D. B. Tanner, C. S. Jacobsen, A. F. Garito, and A. J. Heeger, Phys. Rev. B 13, 3381 (1976).

[8]H. Frohlich, Proc. R. Soc. A 223, 296 (1954); R. E. Peierls, *Quantum Theory of Solids* (Clarendon, Oxford, 1955), p. 108; A. M. Afanas'ev and Yu Kagan, Zh. Eksp. Teor. Fiz. 43, 1456 (1963) [Sov. Phys.-JETP 16, 1030 (1963)]; S. Barisic, Phys. Rev. B 5, 941 (1972); Ann. Phys. (Paris) 7, 23 (1972); L. Gorkov, in *Collective Properties of Physical Systems*, edited by B. Lundquist and S. Lundquist (Academic, New York, 1973); B. Horowitz, H. Gutfreund, and M. Weger, Phys. Rev. B 9, 1246 (1974); J. Bardeen, Solid State Commun. 13, 357 (1973); D. Allender, J. W. Bray, and J. Bardeen, Phys. Rev. B 9, 119 (1974).

[9]F. Denoyer, R. Comes, A. F. Garito, and A. J. Heeger, Phys. Rev. Lett. 35, 445 (1975); S. Kagoshima, H. Anzai, K. Kajimura, and T. Ishigoro, J. Phys. Soc. Jpn. 39, 1143 (1975).

[10]R. Comes, S. M. Shapiro, G. Shirane, A. F. Garito, and A. J. Heeger, Phys. Rev. Lett. 35, 1518 (1975); Phys. Rev. B 14, 2376 (1976).

[11]W. D. Ellenson, R. Comes, S. M. Shapiro, G. Shirane, A. F. Garito, and A. J. Heeger, Solid State Commun. 20, 53 (1976).

[12]G. Shirane, S. M. Shapiro, R. Comes, A. F. Garito, and A. J. Heeger, Phys. Rev. B 14, 2325 (1976).

[13]J. P. Pouget, S. K. Khanna, F. Denoyer, R. Comes, A. F. Garito, and A. J. Heeger, Phys. Rev. Lett. 37, 437 (1976).

[14]S. M. Shapiro, G. Shirane, A. F. Garito, and A. J. Heeger (unpublished).

[15]S. Kagoshima, T. Ishiguro, and H. Anzai, J. Phys. Soc. Jpn. 41, 2061 (1976).

[16]Y. Tomkiewicz, A. R. Taranko, and J. B. Torrance, Phys. Rev. Lett. 36, 751 (1976).

[17]E. Rybaczewski, S. Smith, A. F. Garito, A. J. Heeger, and B. Silbernagel, Phys. Rev. B 14, 2746 (1976).

[18]D. Jerome, W. Muller, and M. Weger, J. Phys. (Paris) 35, L77 (1974).

[19]Per Bak and V. J. Emery, Phys. Rev. Lett. 36, 978 (1976); K. Saub, S. Barisic, and J. Friedel, Phys. Lett. A 56, 302 (1976); A. Bjelis and S. Barisic, in Ref. 2; Phys. Rev. Lett. 37, 1517 (1976).

[20]R. A. Craven, S. Etemad, T. Penney, P. M. Horn, and D. Guidotti (unpublished).

[21]D. Djurek, K. Franulovic, M. Prester, S. Tomic, L. Giral, and J. M. Fabre, Phys. Rev. Lett. 38, 715 (1977).

[22]R. A. Craven, M. B. Salamon, G. Depasquali, R. M. Herman, G. Stucky, and A. Schultz, Phys. Rev. Lett. 32, 769 (1974); A. J. Schultz, G. D. Stucky, R. Craven, M. Y. Schaffman, and M. B. Salamon, J. Am. Chem. Soc. 98, 5191 (1976).

[23]T. D. Schultz and S. Etemad, Phys. Rev. B 13, 4928 (1976).

[24]H. A. Mook and C. R. Watson, Phys. Rev. Lett. 36, 801 (1976).

[25]J. B. Torrance, H. A. Mook, and C. R. Watson (unpublished); H. A. Mook and C. R. Watson (unpublished).

[26]R. Comes, M. Lambert, H. Launois, and H. R. Zeller, Phys. Rev. B 8, 571 (1973); for more details see also B. Dorner and R. Comes, in *Dynamics of Solids and Crystals by Neutron Scattering*, edited by T. Springer (Springer, Berlin, to be published).

[27]H. Morawitz, Phys. Rev. Lett. 34, 1086 (1975); C. Weyl, E. H. Engler, K. Bechgard, G. Jehanno, and S. Etemad, Solid State Commun. 19, 925 (1976); K. Carneiro, Phys. Rev. Lett. 37, 1227 (1976); M. Weger and J. Friedel, J. Phys. (Paris) 38, 241 (1977).

[28]G. Shirane (private communication).

[29]V. J. Emery, Phys. Rev. Lett. 37, 107 (1976); J. B. Torrance (private communication), and in Ref. 2; P. A. Lee, T. M. Rice, and R. A. Klemm, Phys. Rev. B 15, 2984 (1977); L. Sham, Solid State Commun., 20, 623 (1976); H. Sumi, Solid State Commun. 21, 17 (1977); V. J. Emery, in Ref. 2; S. Barisic (unpublished).

[30]A. A. Ovchinnikov, Zh. Eksp. Teor. Fiz. 64, 342 (1973) [Sov. Phys.-JETP 37, 176 (1973)]. J. Bernasconi, M. J. Rice, W. R. Schneider, and S. Strassler, Phys. Rev. B 12, 1090 (1975).

[31]P. Coppens, Phys. Rev. Lett. 35, 98 (1975); W. D. Grobman, R. A. Pollak, D. E. Eastmann, E. T. Maas, Jr., and B. A. Scott, Phys. Rev. Lett. 32, 534 (1974).

[32]J. J. Ritsko, N. O. Lipari, P. C. Gibbons, and S. E. Schnaterly, Phys. Rev. Lett. 37, 1068 (1976).

[33]G. Soda, D. Jerome, M. Weger, J. M. Fabre, L. Giral, and K. Bechgaard, in Ref. 2; E. Ehrenfreund and A. J. Heeger (unpublished).

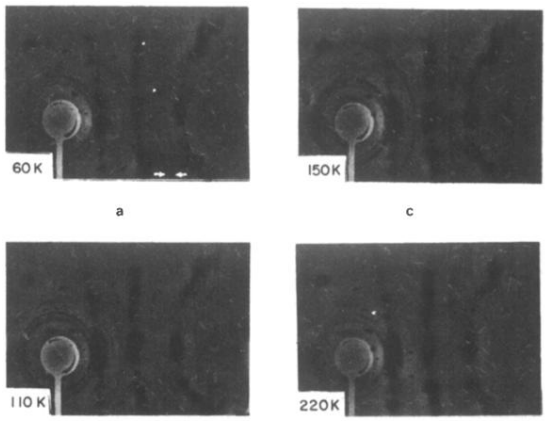

FIG. 1. Diffuse x-ray patterns of TTF-TCNQ in the undistorted conducting phase ($T > 54$ K). The sample is oriented with the b^* and c^* directions in the equatorial plane, the angle between the incident x-ray beam and b^* being 124°. The rings observed around the incident beam are powder parasites from the sample holder. Bragg spots with 0.5 b^* components are due to the $\frac{1}{2}\lambda$ contamination from the continuous spectrum of the x-ray source, which is also reflected by the monochromator. (a) 60 K: The satellite diffuse sheets are clearly visible at the wave vectors $(0.295 \pm 0.02)\, b^*$ identified as $2k_F$ (black arrows) and $(0.59 \pm 0.02) b^*$, the latter corresponding to $0.41 b^*$ in the reduced zone, identified as $4k_F$ (white arrows); (b) 110 K: The $2k_F$ scattering has decreased in intensity and is broadened, whereas the $4k_F$ scattering remains sharp; (c) 150 K: The $2k_F$ scattering is undetectable by eye and only $4k_F$ scattering is visible; (d) 220 K: The $4k_F$ scattering is still clearly visible.

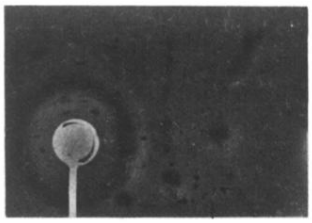

FIG. 10. Diffuse x-ray pattern of TTF-TCNQ at 30 K. The sample is oriented in the reciprocal equatorial plane $(0kl)$, the angle between the incident x-ray beam and b^* axis being 124°. Both the $2k_F$ and the $4k_F$ scatterings are condensed into satellite spots at the wave vectors $(0.25a^*, 0.295b^*, 0c^*)$ and $(0.5a^*, 0.41b^*, 0c^*)$, respectively. Horizontal arrows point toward the $2k_F$ (4.25, 2.295, $\bar{1}$) and (3.75, 2.705, 0) satellites, vertical arrows point toward the $4k_F$ (3.5, 2.41, $\bar{1}$) and (4.5, 2.59, 0) satellites.

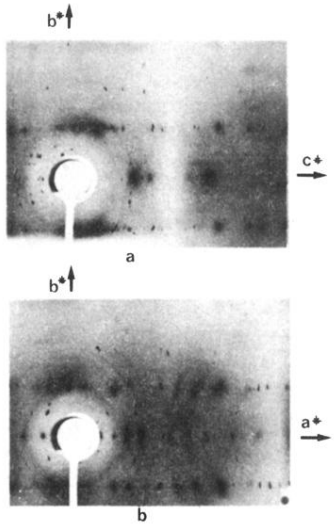

FIG. 7. Diffuse x-ray patterns of TTF-TCNQ taken at 60 K for the two different orientations of Fig. 6. Along the vertical b^* axis [$l = 0$, no c^* component of the scattering vector in Fig. 7(a) and $h = 0$, and no a^* component of the scattering vector in Fig. 7(b)], both the $2k_F$ and $4k_F$ scatterings can be observed showing the existence of a longitudinal component (along b) of the polarization for the $2k_F$, as well as the $4k_F$ scatterings. (a) With increasing l (c^* direction), only the $2k_F$ scattering intensity increases. This is, in particular, striking close to the equatorial layer line where the b^* longitudinal component contributes only negligibly. (b) Neither $2k_F$ nor $4k_F$ scatterings exhibit an increase in intensity for increasing h (along a^*), showing the absence of any substantial a^* component of their polarization.

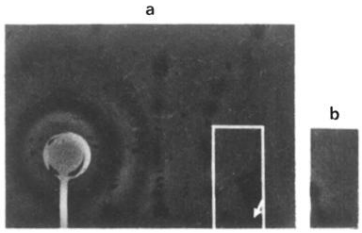

FIG. 9. (a) Diffuse x-ray pattern of TTF–TCNQ at 50 K (modulated phase I). The sample is oriented in the reciprocal equatorial plane $(0kl)$, the angle between the incident x-ray beam and the b axis being 125°. Note that besides the well-defined $2k_F$ arrays of weak satellites with wave-vector components $(0.5a^*, 0.295b^*, 0c^*)$, sharp 1-D $2k_F$ scattering persists at this temperature. The $4k_F$ scattering retains its 1-D character at this temperature (no $4k_F$ satellites). As in the patterns of Fig. 1, Bragg spots with $0.5b^*$ components must be disregarded, as they arise from $\frac{1}{2}\lambda$ contamination. In the insert, the black arrow points toward the (3.5, 3.295, 3) satellite, where the onset of the 3-D order was measured (see Fig. 8), the white arrow points toward the (4.5, 3.295, 5) satellite. (b) The same region as the insert is shown at 55 K, where the two satellites are clearly broadened.